Experimental analysis and simulation of the optical properties of gold nano-particles on sodium alginate

CATERINA SUMMONTE,[1] ALBERTO MAURIZI,[1] RITA RIZZOLI,[1] FABRIZIO TAMARRI,[1] MONICA BERTOLDO,[2,3] GABRIELE BOLOGNINI,[1,*] [iD] AND PIERA MACCAGNANI[1]

[1]*Consiglio Nazionale delle Ricerche, Istituto per la Microelettronica e i Microsistemi, Bologna 40129, Italy*
[2]*Università degli Studi di Ferrara, Dipartimento di Scienze Chimiche, Farmaceutiche ed Agrarie, Ferrara 44121, Italy*
[3]*Consiglio Nazionale delle Ricerche, Istituto per la Sintesi Organica e la Fotoreattività, Bologna 40129, Italy*
*bolognini@bo.imm.cnr.it

Abstract: The reflectance and transmittance spectra of a set of thin gold films on sodium alginate are measured and simulated in the framework of the generalized transfer matrix method. In the simulation, the dielectric function for the nano-particles (NP) was modified from that of gold bulk by using a variable damping energy. A Lorentz oscillator was used to describe the localized surface plasmon resonance. The results elucidate the structural arrangement of the deposited material on the specific substrate. The collision frequency obtained from the simulation indicates that the aggregation of the NPs at the nanoscopic level correlates with the electrical properties. The intense surface plasmon resonance remains visible for film thicknesses up to 10 nm, in spite of the increasing loss of particle separation. In addition to the attained results, the developed methodology can be usefully applied on other case studies for a thorough characterization of the formation of the growing NP films on the specific substrate.

1. Introduction

In opto-electronic applications, when both optically transparent and electrically conductive materials are required, indium tin oxide (ITO) is normally used [1]. This occurs in a wide range of applications that span from light-emitting diodes to photovoltaic cells, touch-sensitive screens or flat panel displays, and many others. Unfortunately, being indium a critical raw material, ITO is becoming increasingly expensive, and the identification for a replacement material would be highly desirable. Moreover, ITO is not suitable for flexible devices, due to its brittle nature. In this framework, the fabrication of thin transparent and conductive films on polymers is becoming an interesting research field for next generation devices for applications such as wearable electronics or soft robotics, where both high flexibility and lightweight are important requisites. Among the different polymers, sodium alginate (SA) is a very interesting material, because it is a cheap, bio-compatible and biodegradable material, derived from brown marine algae, which can be easily used to produce flexible and optically transparent substrates. SA is an insulating polymer, which can be converted to conductive by simply sputtering gold on top, so that a thin surface conductive film with high adhesion is formed [2,3].

When gold is deposited on a substrate by sputtering or evaporation, at the initial stages of deposition the material forms an inhomogeneous layer, which does not retain the properties of the bulk material [4–9]. Isolated regions, or nanoparticles, NP, are formed, with peculiarities that impact on the optical and electrical properties of the growing film. The formation of NPs is likely influenced by surface characteristics of the substrate [10].

It would then be desirable to acquire the knowledge of the details of the deposition process on unconventional substrates, such as SA. Simple, yet sensible techniques such as optical characterization might give rapid insight on the details of the arrangement of the nanometric growing material, and, to this aim, it would be desirable that the optical spectra were supported by suitable simulation, able to derive structural information from the optical peculiarities of the grown material. The interest in gold NP properties dates long ago, as they cover numerous applications in optics, plasmonics, electronics, nanophotonics, sensing, biology, light harvesting, waveguiding, microscopy, biomedicine, and many others (see Refs. [7–8,11–18] for reviews). A wide literature exists, both on the theory of the interaction of nanoparticles with light, which is strongly correlated with dispersion of the nanoparticle shape and size and the overall morphology (see Refs. [7,13,15,17–27] for a not exhaustive review), and on the experimentally determined optical spectra. Most of the attention is devoted to the optical properties of regular and well separated NPs, with narrow size distribution [10,26–33]

On the contrary, little attention has been devoted to the case of more random, irregular and intricate situations, like the early stages of the deposition of thin gold films, before the evolution towards homogeneous thin films, which retain the bulk material properties [5–7]. Only few studies are reported on reflectance and transmittance spectroscopy followed by simulation, in spite of the ability of the technique of supplying non-destructive, routine technological information on the growing material [34].

In most papers, simulations are performed on well separated NPs, with defined shape and size. This is the case of an optical system that can be described with sufficient accuracy using the exact approach based on the Mie theory, and successive modifications that have been developed to account for geometrical peculiarities [4,10,13,18,19,22,24,31,33,35]. If the optical system is accurately described and the correct dielectric functions (DF) for its components are used, the NP-related optical features, such as scattering and extinction, or plasmon signals, are correctly predicted [31]. For this kind of optical systems, the simulation is typically focused on the shape and spectral positions of the plasmon signal that are reproduced by acting on the geometrical parameters of the optical system [35,36]. Consequently, the spectral position of the plasmon signal can be taken as an information itself, which can be used to draw conclusions about the material under investigation, such as NP size and arrangement [8,26,31,32,37].

In all cases, the DF of the NPs is needed for the simulation. Some authors assume the unmodified DF of bulk gold [10,36,38]. Alternatively, a specific DF for NPs is typically obtained using the Drude-Lorentz formulation somewhat derived from that of bulk gold, where a size dependent damping energy [31,33,39] or plasma energy [4,5] or both [18,27] are inserted in the Drude term. However, a bottom-up approach is no longer suitable to treat the case of very thin films, where the irregular arrangement and the dispersion in size, shape, and separation, cannot be longer followed by simulation. In this case, a phenomenological description can still reveal information on the growing material. A treatment based on Fresnel formulas at planar interfaces, or a more comprehensive description such as the scattering matrix method can then be used, [25,40,41], which however can also be applied to the case of ellipsometric spectra of well separated, mono-dispersed NPs [30]. Using this method, a source for the plasmon signal must be introduced in the optical model. A dedicated Lorentz oscillator is a typical choice: a specific layer described by a Lorentz oscillator has been proposed [41]; or a Lorentz oscillator has been introduced in the analytical description of the DF of the NPs [25]. A Lorentz oscillator has been also used to describe the optical system by means of the spectral distribution function [40]. If we stick our review to the simulations of R&T spectra of irregular thin gold films, very little is found in the literature.

The authors in [5], using the simulation of UV vis spectra of thin sputtered films, obtain the plasma frequency and Tauc bandgap of the gold thin film; however, only the fitting parameters are reported in the paper. Reference [42] makes use of Mie theory-based simulation for the R&T

spectra to check the technological process for a solar cell device. In most cases, the reported R&T spectra of low coverage films are directly discussed, yet, only qualitative conclusions are drawn [7,9]. In some cases, the spectra are simply inverted to obtain the extinction coefficient of the film [6]. On the other hand, examples of simulation can be found for spectral ellipsometry taken on thin films [30,40,41].

In summary, we note that the most of the attention so far has been devoted to the comprehension and description of the interaction of light with gold NPs and their arrangement, providing a considerable theoretical and computational apparatus, which however has mostly been applied to studies on material science rather than to the characterization of practical devices.

In this paper, a more phenomenological approach is used. Rather than focusing on modeling aspects, our goal in this work is to apply the optical characterization to gold NP thin films viewed as technological building block layers, which for their nature are characterized by a random, irregular and intricate arrangement, finally enabling the use of spectro-photometric techniques as a routine tool in NP technological processing. Specifically, we intend to investigate the technological details related to the deposition of thin gold films on SA substrate, in view of its many applications, such as in green biocompatible opto-electronic devices. We performed the analysis of random aggregations of dispersed NPs, with different size and shape, using a top-down approach. The film/substrate optical system is described within the framework of the generalized transfer matrix method [43]. The DF of the NPs is analytically described using a Drude-Lorentz approach, where the Drude term contains information of the increased collision frequency. The observed intense Localized Surface Plasmon (LSP) resonance signal is taken into account by means of a specific oscillator. In this approach, the details of individual NPs in term of morphology, size and arrangement are neglected, yet, the features at the nanoscale are revealed from their contribution to the macroscopic properties of the material, through the quantitative simulation of the experimental R&T spectra taken in the range 250-1000 nm, on a set of gold NPs thin films deposited on SA. The collision frequency obtained from the simulation is put in relation to the aggregation of the NPs at the nanoscopic level, and to the electrical properties. The result of the analysis is represented by the DF, and specifically the collision frequency and the LSP parameters, for a set of 14 different samples. To our knowledge, no results of this kind for similar sets of experimental data for gold NPs have been reported before.

2. Experimentals

Flexible, free-standing SA membranes, with thickness of several tens of microns, were prepared by solution casting from 4% wt Alginic Acid Sodium Salt (Sigma-Aldrich) solution in water. The membranes were used as substrates for the deposition of Gold NPs, obtained by RF sputtering at room temperature. The RF plasma power was either 20 or 30 W. Different thicknesses were obtained by varying the deposition time in the range 45-160 s. Optical spectra were obtained by a fiber optics UV-visible Avantes spectro-photometer in the range 300-1100 nm, equipped with an integrating sphere. Great care was taken in measuring reflectance (R) and transmittance (T) spectra at the same sample location. The obtained transmittance spectra were also corrected for the light back-reflected into the sphere. The use of the integrating sphere is dictated by the inherently rough SA substrate, rather than to scattering due to the thin gold film. This was confirmed also by separate measurements taken on bare SA substrates. In principle, the integrating sphere also collects the NP scattered radiation, which is therefore incorrectly ascribed either to reflectance or to transmittance, depending on the scattering angle. However, this aspect is ignored in the calculations because, since gold NP diameter is comparable to the film thickness, practically undetectable scattering is expected [15].

A light beam impinging on the sample at normal incidence was used. For non-spherical particles, only longitudinal plasmon modes (parallel to the sample surface) are excited with this technique. [21,44]. Therefore, our results are focused on this case.

3.   Optical simulations

To simulate the reflectance and transmittance (R&T) spectra we made use of the Generalized Transfer Matrix (GTM) method [43], applied to the film-on-substrate structure. The model also includes the separately determined dielectric function (DF) of the SA material [45]. Briefly, the material shows some absorption at wavelengths up to 400 nm, whereas for longer wavelengths it is transparent with a refractive index of about 1.5. To obtain the DF of gold NPs, we started from the DF of bulk gold described by the implementation of the Drude-Lorentz model, to which the Drude term is modified to account for NP peculiarities, as it is described below.

The Drude-Lorentz analytical form for the imaginary part ε_2 of the various dielectric functions DFs (bulk gold and gold NPs) can be written as:

$$\varepsilon_2(E) = \sum_i \frac{E_{0i}^2 \cdot \Gamma_{Bi} \cdot E \cdot (A_i - 1)}{\left(E_{0i}^2 - E^2\right)^2 + \left(\Gamma_{Bi} \cdot E\right)^2} + \frac{E_P^2 \cdot E_T}{\left(E_T^2 - E^2\right) \cdot E} \tag{1}$$

In the second term on the right hand side (the Drude term), E_P represents the plasma energy and E_T the damping energy, given by $E_T = h\nu_c$, where h is the Planck constant and ν_c is the collision frequency. In the first term of the right-hand side of Eq. (1), the oscillators appearing in the sum are modified from the simple Lorentz form [46] as they feature an energy dependent broadening parameters Γ_{Bi}, defined as:

$$\Gamma_{Bi} = \Gamma_i \cdot \exp\left[-\alpha_i \cdot \left(\frac{E - E_{0i}}{\Gamma_i}\right)^2\right] \tag{2}$$

where α_i is the lineshape parameter. The energy dependent broadening parameter Γ_{Bi}, originally introduced in [47], and later applied to the Lorentz oscillator model [46,48], has been introduced to weaken the contribution of the oscillator for energy values sufficiently different from the oscillator energy [49]. The usual form of the Lorentz oscillator is retained if α_i is set to zero. The other symbols are the oscillator amplitude A_i, and the energy E_{0i}. Once ε_2 is defined, then ε_1 is obtained from ε_2 by means of Kramers-Kronig (KK) transformation. This is needed to guarantee the KK consistency between the real and imaginary part of the dielectric constant, which gets lost if the energy-dependent broadening parameter is used. All calculations are performed using the in-house developed free-ware GTB code [50].

   DF of bulk gold

To obtain the DF of bulk gold, Eq. (1) has been fitted to the experimental spectra of Ref. [51]. In the simulation, the region of inter-band transitions [31] is described by a sum of three modified Lorentz oscillators, whereas the Drude term accounts for free carrier absorption (FCA). All resulting fitting parameters are reported in Table 1.

Table 1. Parameters of Lorentz oscillators for bulk gold[a]

Oscillator	A	E (eV)	Γ (eV)	α
1	2.79 ± 0.04	6.25 ± 0.01	3.81 ± 0.05	2.00[a]
2	3.18	3.97	1.80	1.48 ± 0.05
3	2.21	2.84	0.88	0.78

[a]Parameters were obtained using Eq. (1), (2) fitted over the experimental data of [51]: Amplitude, energy, broadening, and lineshape parameter. The obtained plasma energy and damping energy were $E_{PB} = 8.78 \pm 0.02$ eV and $E_{TB} = 0.073 \pm 0.005$ eV respectively, where B stands for 'bulk gold'. The analytical form is valid in the range 0.62-6.2 eV.
[a]kept fixed in the simulation

For the plasma energy, a value equal to $E_P = 8.78 \pm 0.02$ eV has been obtained, in agreement with similar data reported in the literature [25,27,31,52–54]. For the damping energy, the value

$E_T = 0.073 \pm 0.005$ eV has been obtained, a value also confirmed by several literature results [27,28,31,55]. The analytical form is valid in the range 0.62 to 6.2 eV. We note that the damping energy corresponding to the static collision frequency obtained by electrical measurements [56], namely, 0.138 meV, is not suitable to fit the DF of gold at optical frequencies. This occurs because of the inherent frequency dependence of damping energy [57]. The obtained DF of bulk gold is reported in the Supplement 1, Fig. S1, along with the original data. The result compares well with literature results that use a similar approach, see [54]. A comparison with literature results for the Drude parameters of bulk gold can be found in the SI (Table S1).

DF of gold NP

To describe the DF of gold NPs, the plasma energy in Eq.(1) was fixed to the value of bulk gold, whereas the damping energy E_T is set as a free parameter, to account for the limited mean free path and increased collision frequency, ν_c, of the nanostructures with respect to bulk gold [4,18,20,21,26,28,31,33]. The increase of the Drude damping energy E_T for gold NPs is related to the inverse of particle dimensions, possibly through a factor which depends on environment and geometry [17,18,28,33]. Other factors are the scattering of electrons at the NP surface, the interaction of oscillating electrons with other electrons and fixed positive charge, and the energy dissipation within the metallic lattice [18]. The modified oscillators 1 to 3 of Eq. (1), which describe the UV-blue region of the absorption spectrum, dominated by inter-band transitions, have the same parameter values used for bulk gold. Moreover, a fourth oscillator was introduced to account for the strong absorption signal detected in the range 500-1100 nm for film thicknesses below ∼7 nm. This signal is due to the LSP that sets up in presence of isolated gold NPs [15,17,21,22]. Its modeling by means of a Lorentz oscillator was already proposed [25,41]. To conclude this section, the simulation of the DF for gold NP is performed using 5 parameters: the four parameters related to the modified LSP oscillator (E_{LSP}, Γ_{LSP}, A_{LSP}, α_{LSP}, which represent the energy, amplitude, broadening, and line-shape parameter respectively) and the damping energy E_T, for which a lower limit was set equal to the value obtained for bulk gold, E_{TB}. Film and substrate thicknesses were also left as free parameters in the simulation. The possibility of using an effective medium with a void fraction for the gold thin film was not considered in the model used, for reasons that are described in Section 4.

4. Results

The irregular and disordered character of the Au/polymer films, that would be difficult to describe using a bottom-up approach, emerges from SEM images (Fig. 1). The observed roughness is to be ascribed to the organic substrate rather than to the thin gold film [3].

The metallic films appear as an aggregate of NPs, increasingly interconnected for growing thicknesses. For the thinnest sample (2.0 nm from the simulation, see below), a clearly discontinuous layer is observed (Fig. 1(a)). This would suggest that the material could be properly simulated using an effective medium approximation, with the introduction of a void fraction. However, this was not applied because, for thicknesses much lower than the onset of interference as in this case, thickness and void fraction are correlated parameters that cannot be simultaneously determined. The thickness extracted from the simulation is therefore the lower limit of the actual thickness, and, in presence of a low-density material, is to be regarded as an "equivalent" thickness, i.e., the thickness of a dense film containing the same amount of material.

From the optical simulation, film thicknessess in the range 2.0 to 26.5 nm are obtained. The experimental R&T spectra, as well as the spectra resulting from simulations, are reported in Fig. 2. The arrows indicate the direction of increasing film thickness. The sample with highest R and lowest T refers to a 26.5 ± 1.5 nm thick Au sample. For this sample, the best fit converged to the optical constants of bulk gold, i.e., A_{LSP} vanished, whereas E_T saturated at its minimum allowed value, namely, the value of bulk gold.
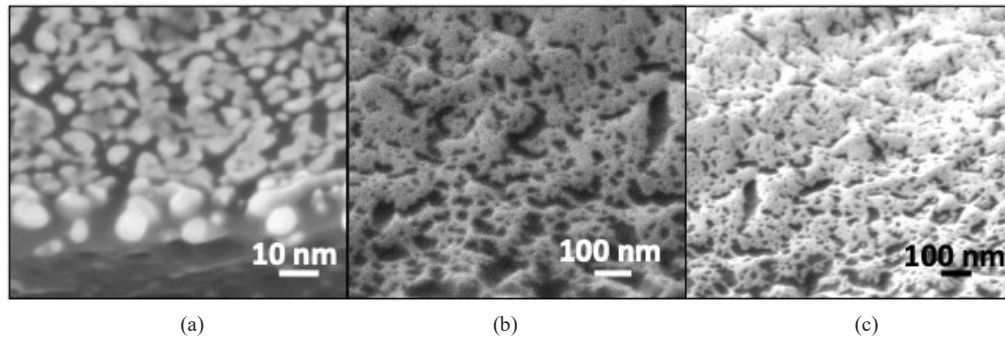
Fig. 1. SEM images of selected gold/SA films, with deposition conditions and simulated thickness, from left to right: (a) 20 W, 45 s, 2.0 ± 0.5 nm; (b) 30 W, 75 s, 3.4 ± 1.0 nm; (c) 20W, 90 s, 3.5 ± 1.0 nm. The observed roughness is to be ascribed to the organic substrate rather than to the thin gold film.
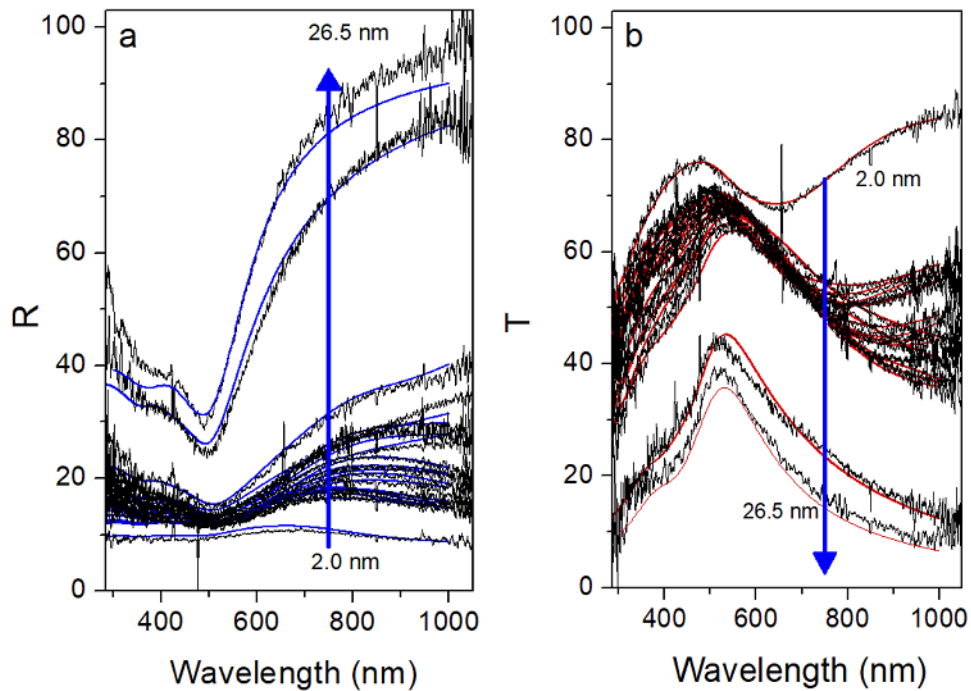

Fig. 2. (a) Experimental (black) and calculated (color) reflectance for all samples. The arrows indicate the direction of increasing overall deposited material. (b) Experimental (black) and calculated (color) transmittance for all samples. The arrows indicate the direction of increasing overall deposited material.

An overall good agreement for all samples between experimental and simulated spectra is shown in Fig. 2, confirming the validity of the developed optical model. In Fig. 2(b), most spectra exhibit a broad minimum in T, located at around 650 nm for the 2 nm sample, and at longer wavelengths for thicker samples. Such a minimum, which cannot be simulated using the DF of bulk gold in the framework of the GTM method, indicates the presence of the intense extinction signal associated to the onset of LSP resonance. Because of the lower sensitivity of R on absorption, the same feature is less evident in R spectra.

We now focus on the parameters obtained from simulations. The equivalent thickness of gold films is reported in Fig. 3. The figure shows a constant (equivalent) deposition rate, higher for higher plasma power in RF sputtering deposition. The obvious result supports the choice for the optical model. Figure 4(a), 4(b) report the energy and broadening of the LSP oscillator as a function of equivalent film thickness. The LSP energies (Fig. 4(a)) are located in the range between 1.2 and 1.8 eV; we can observe a decrease in E_{LPS} for increasing film thicknesses up to $\sim$ 5 nm, while for thicker films the red shift behaviour is not maintained. The contribution of the LSP to the imaginary part of the DF, $\varepsilon_{2,LSP}$, is calculated from Eq. (1) by ignoring the Drude term, and inserting only the LSP term in the sum. Figure 4(c) shows that the $\varepsilon_{2,LSP}$ peak intensity (i.e. $\varepsilon_{2,LSP}$ at $E = E_{LSP}$) increases as the film thickness increases from 2 nm to $\sim$ 4 nm, then it decreases, vanishing at $\sim$ 10 nm.
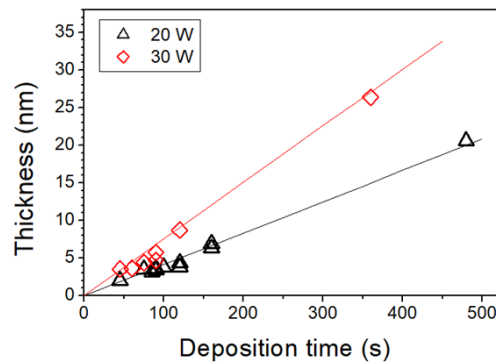

Fig. 3. Equivalent thickness obtained from the simulation of experimental R&T spectra. The legend indicates the plasma power used for the sputtering deposition process (triangles: 20W power, diamonds: 30 W power). The lines indicate a linear fitting.

The spectral $\varepsilon_{2,LSP}$ for all samples are reported in the SI, Fig. S3. The overall behaviour (initial increase with thickness associated with some red shift, then a decrease of intensity with no further shift in energy), is also evident. All LSP parameters are reported in Table S1 of SI.

In Fig. 2(a), and 2(b), we note that the simulation quantitatively covers the experimental spectrum from the region of interband transitions (wavelengths between 300 to about 500 nm) to the near infrared region ($\approx$ 1000 nm wavelength), not only on the LSP resonance region. It is for this reason that the collision frequency could be obtained as an independent parameter and encompassed within its mathematical description, rather than its effect being confused with the details of the LSP.

Hence, an insight on NP aggregation can be obtained from the collision frequency obtained from the damping energy E_T as $\nu_c = E_T / h$. E_T for all samples is reported in Table S1 of the SI. The collision frequency is reported in Fig. 5 as a function of film thickness. In the figure, the experimental points are arranged along a narrow line with minimum scattering, which again supports the validity of optical model employed in the simulations and the physical significance of the fitting parameters. The figure shows that the collision frequency is sensibly higher than the 'bulk' value, $\nu_{c,BULK} = E_{TB}/h$, also reported in the figure.
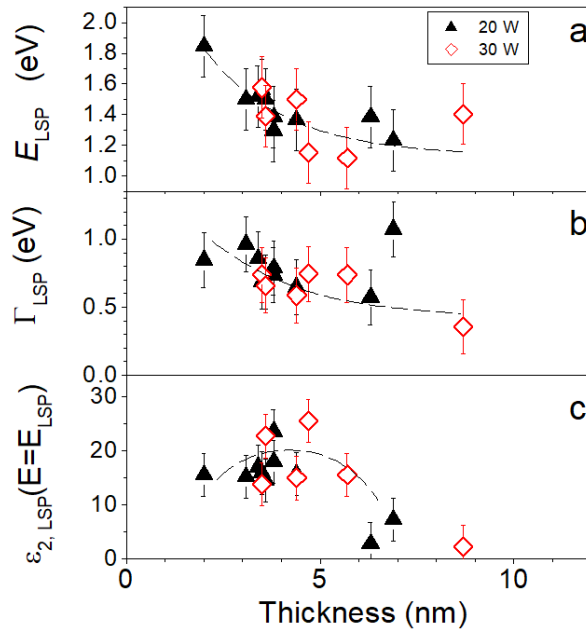
Fig. 4. LSP parameters as a function of equivalent thickness: energy of the LSP oscillator, E_{LSP} (a); broadening of the oscillator, Γ_{LSP} (b); peak value of the associated contribution to the imaginary part of the dielectric constant, $\varepsilon_{2,LSP}$ (c). The lines are a guide to the eye. (triangles: 20W power, diamonds: 30 W power)
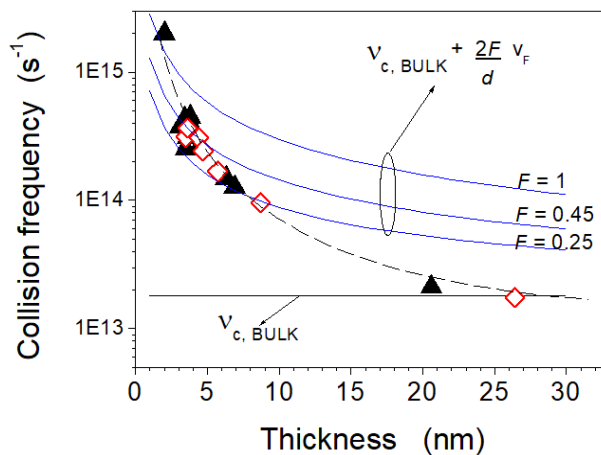

Fig. 5. Collision frequency versus equivalent thickness of samples (triangles. The value for bulk gold is also indicated. The continuous lines represent the condition of thickness-dependent mean free path Eq. (3), for some of the different values of the fitting factor F that can be found in the literature. The dashed line is a guide for the eye. (triangles: 20W plasma power, diamonds: 30 W plasma power)

For our reference, we can compute the collision frequency of isolated NPs of diameter d, which is given by Eq. (3):

$$v_c = v_{c,\ BULK} + \frac{2V_F}{d} \cdot F \tag{3}$$

where $v_F = 1.4 \cdot 10^{15}$ nm/s is the Fermi velocity for gold and F is an empirical fitting parameter [15,17,18,20,26,28,31].

If we set d equal to the film thickness, Eq. (3) also represents the expected collision frequency for electrons scattered at the surface of gold NPs having a diameter equal to the film thickness.

Equation (3) is plotted in Fig. 5 for different values of F, which is often assumed equal to 1, although values from 0.1 to 2 have been reported [17]. With reference to such curves, we observe that at the very initial stages of the deposition, and under our experimental conditions, the obtained v_c is consistent with isolated NPs with diameter comparable to the film thickness. For higher thicknesses, v_c rapidly decreases, becoming equal to $v_{c,BULK}$ when the thickness reaches 20 nm, hence indicating that in-plane aggregation and interconnection of the deposited material has occurred, so that the contribution of the interaction of optically excited carriers with NP surfaces becomes negligible.

A comparison between the results of Figs. 4 and 5 indicates a strict correlation between the LSP details and the collision frequency. It is observed that the LSP amplitude decreases for increasing film thickness, and vanishes when, based on the optically extracted collision frequency, the deposited material approaches the bulk limit.

The optical analysis also motivates the results of the electrical characterization that we performed for our manufactured devices, that have been partially reported in a previous paper [3]. The sheet resistance (vs sample thickness) measurements are reported in Fig. 6.
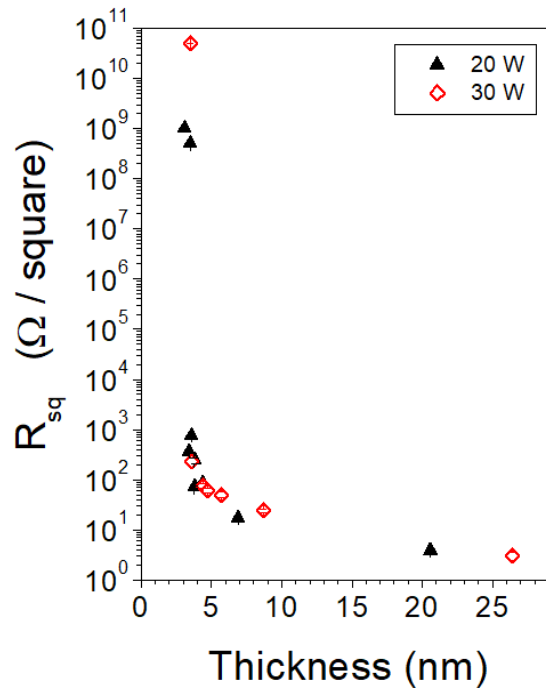

Fig. 6. Sheet resistance measured on manufactured samples, vs. equivalent thickness (triangles: 20W plasma power in sputtering deposition, diamonds: 30 W plasma power in sputtering deposition).

Both optical and electrical measurements confirm the evolution towards an isolated NP model for decreasing thickness of deposited material. Specifically, an increase in sheet resistance of several orders of magnitudes is observed for both values of RF plasma power when film thickness decreases below ∼4 nm (see Fig. 6). With reference to Fig. 5, as noted above, for such a low thickness the collision frequency is compatible with the case of isolated NPs, although a precise threshold value for the occurrence of continuous domains is uncertain due to the controversial values of the empirical factor F reported in the literature. In other words, as soon as an electrical percolation network starts forming in the growing gold layers, an effect is optically detected in the decrease of the collision frequency. Yet, the presence of a LSP still persists (Fig. 4. and Table S1), indicating some presence of isolated gold NPs, which progressively decrease in abundance (Fig. 4(c)), and eventually become non-significant for the thickest samples. The results of optical simulations are also in quantitative agreement with noise spectroscopy experiments taken on similar samples, which have been reported in [58].

In fact, it is reported that below a certain gold layer thickness, identified by the authors in [54] in 4.5 nm, the ultrathin films feature a network of discontinuous metallic regions, whose morphology results in specific non-metallic features. For larger thicknesses, the conducting regions are more uniformly distributed and interconnected [58]. Our results show the existence of a smooth transition between the cases studied in the reported reference.

Finally, Figs. 4 to 6. also show that, under the investigated conditions, no evidence is observed of an impact of the different plasma power values in the deposition process. At least for the short deposition times used, the higher deposition rate observed for 30 W plasma power (Fig. 1) does not seem to be sufficient to sensibly affect NP separation, as predicted in Ref. [8].

5.   Discussion

In section 4 we have reported the simulation of R&T spectra for a set of very thin, sputter-deposited gold films on SA substrate. The free parameters in the simulations are the film and SA thickness, the four parameters of the LSP Lorentz oscillator, and the damping energy in the Drude term, whereas the plasma energy is kept at the value of bulk gold.

With reference to the energy position of the LSP band and the related red shift for increasing Au thickness (Fig. 4(a)), similar conclusions can be deduced from a visual inspection of transmittance or absorption spectra reported in the literature for evaporated or sputtered thin gold films [5–7,9]. The energy values we observe are lower than the value of about 2 eV predicted for mono-dispersed, isolated gold NPs with diameters up to at least 100 nm, with only a slight red shift for increasing diameter [26,28], and with the exact value also depending on shape, separation, and dielectric environment [21,23,25,27,28].

Note that a large broadening (Γ_{LSP}) has been observed in our study, (Fig. 4(b)). Large broadenings have been related in literature to the shape of NPs [18] or to phase retardation [59]. In our case, however, since we are dealing with a random aggregation of NPs, the spectral LSP width is likely dominated by the distribution of NP size, shape, as well as isolation, rather than by the peculiarities of the LSP related to a single NP [8].

For non-spherical NPs, a red shift of LSP resonance has been also correlated to increased NP ellipticity [8,60]. Hence, the low oscillator energy and the large broadening obtained (Fig. 4(a),(b)) are rather indicative of an irregular set of elongated structures, that exhibit a longitudinal mode oscillating along the longer direction, located at a red-shifted wavelength according to the aspect ratio [8,22,39,60]. However, a numerical calculation was not attempted for our data because the argued dispersion in shape and sizes would make the determination of an aspect ratio from the numerical fit of the data reported in Fig.4a too speculative.

The amplitude of the LSP shows an initial increase with thickness (Fig.4c), as expected for isolated NPs [13], followed by a decrease, and complete vanishing for thicknesses above 10 nm

(Fig.4c), which in turn is no longer compatible with isolated NPs, since the LSP signal in that case is expected to persist to much bigger diameters [17].

We attribute the observed reduction to the increasing formation of electrical percolation paths between previously separated domains, that results in LSP coupling and consequent quenching [7,61]. For the largest Au thicknesses, a continuous film is formed. This scenario is also supported by the decrease of the collision frequency with thickness (Fig. 5), which follows a decreasing rate which is more rapid than expected for isolated NPs having diameter similar to the film thickness, regardless of the value of the fitting parameter F one would consider correct in our case.

The interruption of the red shift of the LSP energy (Fig.4a), associated with the decrease of intensity (Fig.4c) and of broadening (Fig.4b), is compatible with the scenario where the observed LSP resonance is due to the convolution of a family of signals [8,10], originated from sub-regions where the NPs have similar shape and size dispersion, and which become less populated as thickness increases. As the quantity of deposited material increases, an increasing number of NPs loses its character of sufficient isolation, with the elimination of the related contribution to the LSP signal.

Finally, we note that since the LSP oscillator is inserted within the DF of gold NPs, the related absorption is treated in the simulations as a volume rather than a surface property, which would be more correct for localised plasmon resonance. Thus, given that for increasing NP diameter the volume increases more rapidly than surface, the apparent decrease of $\varepsilon_{2,LSP}$ (Fig. 4(c)) is probably overestimated. Nonetheless, it is confirmed that the decreasing trend proceeds continuously up to the complete disappearance of the absorption band, which, as mentioned above, is no longer detected for the largest thickness, for which the fitting fully eliminates the LSP contribution.

To summarize this section, the optical analysis permits to follow the evolution toward aggregation of an initially inhomogeneous ensemble of irregular, separated nanoparticles, indicating the thickness range in which this occurs for the experimental conditions under investigation.

We stress the peculiarity of the proposed procedure, that allows us to separately obtain information on the arrangement of NPs, (and in particular the smooth transition from separated to interconnected, as indicated both by the collision frequency and the amplitude of the LSP), and on carrier concentration. The latter is found to be consistent with the value for bulk gold, as indicated by the plasma energy of the Drude term, which is successfully fixed at the value of bulk gold, a choice that resulted in a very good fitting for the entire set of samples. Therefore, the limitation to electrical conduction at low film thickness (Fig. 6) is to be related to NP separation rather than to low carrier concentration, in contrast to what observed in Ref. [5], where a decreased plasma energy, and hence carrier concentration, is observed for very low Au thicknesses. It should be noted that the opposite trend, i.e. an increase of plasma energy for decreasing thickness (up to 9.576 eV for thickness decreasing down to 3.6 nm), was obtained by fitting the experimental LSP frequency in the framework of Mie theory [27].

The reported results are related to the specific SA substrate. Given the organic and soft nature of the polymeric substrate, partial Au NP embedding occurs during the deposition process [62]. This embedding in an insulating matrix is likely to have a role in determining the initial level of NP separation, that in turn may be controlled by means of deposition parameters. Indeed, it has been reported in Ref. [63] that for similar deposition conditions, the different substrate roughness (PTE and PTFE in that case) impacts on the conductivity of the final thin gold film, and it is proposed that a higher roughness hinders the creation of a continuous film. The procedure can also be used to conduct a quantitative check over the impact of the specific deposition technique. In fact, it has been shown that, using sputtering, the LSP band is visually broader and at lower energies with respect to the case of thermal evaporation. [6].

For gold NPs on SA substrate, we observed that the convolution of individual LSP signals associated to a certain size, shape, and spacing dispersion of NPs can be described by a modified

Lorentz oscillator. This is not necessarily the case when analysing other substrates. In fact, different substrates might induce different arrangement of the NPs, resulting in a different overall LSP signal shape, so that a different analytical function may result to be more appropriate than the Lorentz oscillator used in our model. The details of such a function for different substrates, such as glass compared to organic (or the same material but different roughness), might provide information that can be used to associate the substrate specific physicochemical properties (nature of the exposed atoms and their structure arrangement, nano-porosity, surface energy, surface viscoelasticity, etc.) to the very initial stages of the growth, in a quantifiable way.

Finally, note that the case study reported here refers to R&T measurements at normal incidence, that are not able to detect features like anisotropy in the DF, or in the NP arrangement, originating for instance from angular deposition of metal NP [64].

However, if a more powerful experimental set up is used, such as for instance Mueller Matrix Ellipsometry [65], or polarized reflectometry [66] associated to a suitable theoretical description framework, the DF model of the material under investigation can still be described as proposed in this paper when fitting the experimental results. Authors in Ref. [64] also reported a similar outcome for their case of anisotropic DF in highly oriented silver NPs, which was described by means of the sum of four oscillators.

The results reported in this paper elucidate details at the nanoscale on the formation of gold-on-sodium alginate material, which has been proposed as transparent, environmentally friendly substrate for flexible electronics [45]. Organic optoelectronic devices require precise control of the optical properties of the substrate, together with its electrical behavior. The developed methodology permitted a comprehension of material aggregation on the polymeric substrate, enabling the fine tailoring of device performance and limiting the thickness of the deposited metal layer at the minimum level for conduction, which has been shown to be as low as 6 nm, yet not associated to the structural peculiarities of bulk gold. This will guarantee low fabrication costs, light weight, and good mechanical flexibility.

6. Summary and conclusion

In summary, we have reported the optical analysis of a set of ultrathin gold films on SA membranes, showing that the measured R&T spectra can be properly simulated by the Drude-Lorentz model, modified from that of bulk gold by leaving the damping energy in the Drude term vary as a free parameter, and introducing the LSP oscillator. This simple picture shows to be very suitable to quantitatively fit a set of as many as 14 experimental spectra, which, to the best of our knowledge, has not been reported to date, and is therefore very powerful to elucidate details such as the thicknesses at which the aggregation of gold NPs takes place on this specific substrate. Specifically, at the early stages of the deposition process, we observe the formation of non-continuous material aggregates. However, an articulated reorganization and interconnection of the deposited material proceeds rapidly. In fact, already at 10 nm thickness does the LSP almost disappear, and beyond 20 nm the peculiarities of a continuous gold film are detected. These results obtained from optical simulations give a reason for the observed electrical behavior of the material, thus supplying a simple tool to evaluate the impact of experimental parameters on the final electrical behavior. In the event that the chemical details of the surface have an impact on the observation, we have indicated an analytical tool to investigate the growth process at the nanoscale. The procedure is suitable to investigate the morphology and the electrical properties of nanometric metallic layers deposited on transparent polymeric substrates, and to explore how the aggregation phenomena of metal NPs at the metal-polymeric interface are affected by the deposition conditions and by different morphologies and nature of the polymeric substrate.

References

1. H. E. Shin, C. O. Jeong, and J. Song, "Metal lines and ITO PVD," in: *Flat Panel Display Manufacturing*, J. Souk, S. Morozumi, F.-C. Luo, and I. Bita eds., (John Wiley & Sons, 2018).
2. C. Barone, M. Bertoldo, R. Capelli, F. Dinelli, P. Maccagnani, N. Martucciello, C. Mauro, and S. Pagano, "Electric transport in gold-covered sodium–alginate free-standing foils," Nanomaterials **11**(3), 565 (2021).
3. P. Maccagnani, M. Bertoldo, F. Dinelli, M. Murgia, C. Summonte, L. Ortolani, G. Pizzochero, R. Verucchi, C. Collini, and R. Capelli, "Flexible conductors from brown algae for green electronics," Adv. Sustainable Syst. **3**, 1–7 (2019).
4. C. G. Granqvist and O. Hunderi, "Optical properties of ultrafine gold particles," Phys. Rev. B **16**(8), 3513–3534 (1977).
5. J. Siegel, O. Lyutakov, V. Rybka, Z. Kolská, and V. Švorčík, "Properties of gold nanostructures sputtered on glass," Nanoscale Res. Lett. **6**(96), 1–9 (2011).
6. A. Axelevitch, B. Gorenstein, and G. Golan, "Investigation of optical transmission in thin metal films," Phys. Procedia **32**, 1–13 (2012).
7. D. Gaspar, A. C. Pimentel, T. Mateus, J. P. Leitão, J. Soares, B. P. Falcão, A. Araújo, A. Vicente, S. A. Filonovich, H. Águas, R. Martins, and I. Ferreira, "Influence of the layer thickness in plasmonic gold nanoparticles produced by thermal evaporation," Sci. Rep. **3**(1), 1469 (2013).
8. V. N. Rai, A. K. Srivastava, C. Mukherjee, and S. K. Deb, "Localized surface plasmon resonance and refractive index sensitivity of vacuum-evaporated nanostructured gold thin films," Indian J Phys **90**(1), 107–116 (2016).
9. S.M. Novikov, J. Beermann, C. Frydendahl, N. Stenger, V. Coello, N. Asger Mortensen, and S.I. Bozhevolnyi, "Enhancement of two-photon photoluminescence and SERS for low-coverage gold films," Opt. Express **24**(15), 16743 (2016).
10. F. Hubenthal, D. Blázquez Sánchez, and Frank Träger, "Determination of morphological parameters of supported gold nanoparticles: comparison of AFM combined with optical spectroscopy and theoretical modeling versus TEM," Appl. Sci. **2**(3), 566–583 (2012).
11. S.A. Maier and H.A. Atwater, "Plasmonics: Localization and guiding of electromagnetic energy in metal/dielectric structures," J. Appl. Phys. **98**(1), 011101 (2005).
12. H.A. Atwater and A. Polman, "Plasmonics for improved photovoltaic devices," Nat. Mater. **9**(3), 205–213 (2010).
13. M. A. Garcia, "Surface plasmons in metallic nanoparticles: fundamentals and applications," J. Phys. D: Appl. Phys. **44**(28), 283001 (2011).
14. M.A. Green and S. Pillai, "Harnessing plasmonics for solar cells," Nat. Photonics **6**(3), 130–132 (2012).
15. X. Fan, W. Zheng, and D.J. Singh, "Light scattering and surface plasmons on small spherical particles," Light: Sci. Appl. **3**(6), e179 (2014).
16. C. Leong Tan, S. Jun Jang, Y. Min Song, K. Alameh, and Y. Tak Lee, "Bimetallic non-alloyed NPs for improving the broadband optical absorption of thin amorphous silicon substrates," Nanoscale Res. Lett. **9**(1), 181 (2014).
17. V. Amendola, R. Pilot, M. Frasconi, O. M. Maragò, and M.A. Iatì, "Surface plasmon resonance in gold nanoparticles: a review," J. Phys.: Condens. Matter **29**(20), 203002 (2017).
18. A. Kheirandish, N.S. Javan, and H. Mohammadzadeh, "Modified Drude model for small gold nanoparticles surface plasmon resonance based on the role of classical confinement," Sci. Rep. **10**(1), 6517 (2020).
19. G. Mie, "Beiträge zur Optik trüber Medien, speziell kolloidaler Metallösungen," Ann. Phys. (Berlin, Ger.) **330**(3), 377–445 (1908).
20. U. Kreibig and M. Vollmer, *Optical Properties of Metal Clusters* 25, Vol. 25 of Springer Series in Materials Science (Springer, Berlin, Heidelberg, 1995).
21. C. F. Bohren and D.R. Huffman, *Absorption and Scattering of Light by Small Particles*, 1st ed. (Wiley, 1998).
22. K. Lance Kelly, E. Coronado, Lin Lin Zhao, and G.C. Schatz, "The optical properties of metal nanoparticles: the influence of size, shape, and dielectric environment," J. Phys. Chem. B **107**(3), 668–677 (2003).
23. C. Noguez, "Surface plasmons on metal nanoparticles: the influence of shape and physical environment," J. Phys. Chem. C **111**(10), 3806–3819 (2007).
24. F. Ruffino, G. Piccitto, and M. G. Grimaldi, "Simulations of the light scattering properties of metal/oxide core/shell nanospheres," J. Nanoscience **2014**, 1–11 (2014).
25. D. Sikdar and A.A. Kornyshev, "Theory of tailorable optical response of two-dimensional arrays of plasmonic nanoparticles at dielectric interfaces," Sci. Rep. **6**(1), 33712 (2016).
26. W. Haiss, N.T.K. Thanh, J. Aveyard, and D.G. Fernig, "Determination of size and concentration of gold nanoparticles from UV-vis spectra," Anal. Chem. **79**(11), 4215–4221 (2007).

27. S. Karimi, A. Moshaii, S. Abbasian, and M. Nikkhah, "Surface plasmon resonance in small gold nanoparticles: introducing a size-dependent plasma frequency for nanoparticles in quantum regime," Plasmonics **14**(4), 851–860 (2019).

28. Stéphane Berciaud, Laurent Cognet, Philippe Tamarat, and Brahim Lounis, "Observation of intrinsic size effects in the optical response of individual gold nanoparticles," Nanoletters **5**(3), 515–518 (2005).

29. C. Humbert, O. Pluchery, E. Lacaze, A. Tadjeddine, and B. Busson, "Optical spectroscopy of functionalized gold nanoparticles assemblies as a function of the surface coverage," Gold Bull. **46**(4), 299–309 (2013).

30. R.S. Moirangthem, M.T. Yaseen, P.-K. Wei, J.-Y. Cheng, and Y.-C. Chang, "Enhanced localized plasmonic detections using partially-embedded gold nanoparticles and ellipsometric measurements," Biome. Opt. Express **3**(5), 899–910 (2012).

31. A. Derkachova, K. Kolwas, and I. Demchenko, "Dielectric function for gold in plasmonics applications: size dependence of plasmon resonance frequencies and damping rates for nanospheres," Plasmonics **11**(3), 941–951 (2016).

32. J. Piella, N.G. Bastús, and V. Puntes, "Size-controlled synthesis of sub-10-nanometer citrate-stabilized gold nanoparticles and related optical properties," Chem. Mater. **28**(4), 1066–1075 (2016).

33. A. Centeno, "Improved Drude-Lorentz dielectric function for gold nanospheres," arXiv:2012.05090 [2020].

34. C. Summonte, "Dielectric function and spectrophotometry: from bulk to nanostructures," in *Light Energy Harvesting with Group-IV Nanostructures*, J. Valenta and S. Mirabella eds., (Pan Stanford Pub., 2015).

35. L.B. Scaffardi and J.O. Tocho, "Size dependence of refractive index of gold nanoparticles," Nanotechnology **17**(5), 1309–1315 (2006).

36. D. Grynko, K. Grytrsenko, V. Lozovski, M. Sopinskyy, and G. Strilchuk, "Optical Absorption of Nano-Composite of Au in Teflon Thin Films," Mater. Sci. Applications **1**, 141–151 (2010).

37. T. Ung, L.M. Liz-Marzán, and P. Mulvaney, "Gold nanoparticle thin films," Colloids Surf., A **202**(2-3), 119–126 (2002).

38. F. Hao and P. Nordlander, "Efficient dielectric function for FDTD simulation of the optical properties of silver and gold nanoparticles," Chem. Phys. Lett. **446**(1-3), 115–118 (2007).

39. V. Amendola and M. Meneghetti, "Size evaluation of gold nanoparticles by UV-vis spectroscopy," J. Ohys. Chem. C **113**(11), 4277–4285 (2009).

40. C. Pecharroman, E. Della Gaspera, A. Martucci, R. Escobar-Galindod, and Paul Mulvaney, "Determination of the Optical Constants of Gold Nanoparticles from Thin-Film Spectra," J. Phys. Chem. C **119**, 9450–9459 (2015).

41. M. M. Giangregorio, M. Losurdo, A. Sacchetti, P. Capezzuto, and G. Bruno, "Plasma processing of the Si(001) surface for tuning SPR of Au/Si-based plasmonic nanostructures," J. Lumin. **121**(2), 322–326 (2006).

42. M. Mendes, S. Morawiec, I. Crupi, F. Simone, and F. Priolo, "Colloidal self-assembled nanosphere arrays for plasmon-enhanced light trapping in thin film silicon solar cells," Energy Procedia **44**, 184–191 (2014).

43. E. Centurioni, "Generalized matrix method for calculation of internal light energy flux in mixed coherent and incoherent multilayers," Appl. Opt. **44**(35), 7532–7539 (2005).

44. M. Losurdo, M. Bergmair, G. Bruno, D. Cattelan, C. Cobet, A. De Martino, K. Fleischer, Z. Dohcevic-Mitrovic, N. Esser, M. Galliet, R. Gajic, D. Hemzal, K. Hingerl, J. Humlicek, R. Ossikovski, Z.V. Popovic, and O. Saxl, "Spectroscopic ellipsometry and polarimetry for materials and systems analysis at the nanometer scale: state-of-the-art, potential, and perspectives," J. Nanopart. Res. **11**(7), 1521–1554 (2009).

45. M. Cocchi, M. Bertoldo, M. Seri, P. Maccagnani, C. Summonte, S. Buoso, G. Belletti, F. Dinelli, and R. Capelli, "Fully Recyclable OLEDs built on a Flexible Biopolymer Substrate," ACS Sustainable Chem. Eng. **9**(38), 12733 (2021).

46. A.D. Rakić and M. L. Majewski, "Modeling the optical dielectric function of GaAs and AlAs: Extension of Adachi's model," J. Appl. Phys. **80**(10), 5909–5914 (1996).

47. C.C. Kim, J.W. Garland, H. Abad, and P.M. Raccah, "Modeling the optical dielectric function of semiconductors: Extension of the critical-point parabolic-band approximation," Phys. Rev. B **45**(20), 11749–11767 (1992).

48. A. B. Djurišić and E. H. Li, "Modeling the index of refraction of insulating solids with a modified Lorentz oscillator model," Appl. Opt. **37**(22), 5291–5297 (1998).

49. C. Summonte, M. Allegrezza, M. Canino, M. Bellettato, and A. Desalvo, "Analytical expression for the imaginary part of the dielectric constant of microcrystalline silicon," Res. Appl. Mater. **1**(2), 6–11 (2013).

50. M. Allegrezza, F. Gaspari, M. Canino, M. Bellettato, A. Desalvo, and C. Summonte, "Tail absorption in the determination of optical constants of silicon rich carbides," Thin Solid Films **556**, 105–111 (2014).

51. P. Johnson and R. Christy, "Optical constants of noble metals," Phys. Rev. B **6**(12), 4370–4379 (1972).

52. B.R. Cooper, H. Ehrenreich, and H.R. Philipp, "Optical properties of noble metals. II," Phys. Rev. **138**(2A), A494–A507 (1965).

53. P.G. Etchegoin, E.C. Le Ru, and M. Meyer, "An analytic model for the optical properties of gold," J. Chem. Phys. **125**(16), 164705 (2006).

54. R.L. Olmon, B. Slovick, T.W. Johnson, D. Shelton, S.-H. Oh, G.D. Boreman, and M.B. Raschke, "Optical dielectric function of gold," Phys. Rev. B **86**(23), 235147 (2012).

55. C. Novo, Dl Gomez, J. Perez-Juste, Z. Zhang, H. Petrova, M. Reismann, P. Mulvaney, and G. V. Hartland, "Contributions from radiation damping and surface scattering to the linewidth of the longitudinal plasmon band of gold nanorods: a single particle study," Phys. Chem. Chem. Phys. **8**(30), 3540–3546 (2006).

56. N.W. Ashcroft and N.D. Mermin, *Solid State Physics*, 1ˢᵗ ed., (Saunders College Publ., 1976).
57. S.R. Nagel and S.E. Schnatterly, "Frequency dependence of the Drude relaxation time in metal film," Phys. Rev. B **9**(4), 1299–1303 (1974).
58. C. C. Barone, P. Maccagnani, F. Dinelli, M. Bertoldo, R. Capelli, M. Cocchi, M. Seri, and S. Pagano, "Electrical conduction and noise spectroscopy of sodium-slginate gold-covered ultrathin films for flexible green electronics," Sci. Rep. **12**(1), 9861 (2022).
59. N.K. Grady, N.J. Halas, and P. Nordlander, "Influence of dielectric function properties on the optical response of plasmon resonant metallic nanoparticles," Chem. Phys. Lett. **399**(1-3), 167–171 (2004).
60. S. Link, M.B. Mohamed, and M.A. El-Sayed, "Simulation of the optical absorption spectra of gold nanorods as a function of their aspect ratio and the effect of the medium dielectric constant," J. Phys. Chem. B **103**(16), 3073–3077 (1999).
61. Xingyou Lang, Lihua Qian, Pengfei Guan, Jian Zi, and Mingwei Chen, "Localized surface plasmon resonance of nanoporous gold," Appl. Phys. Lett. **98**, 1–3 (2011).
62. R. Capelli, P. Maccagnani, F. Dinelli, M. Murgia, M. Bertoldo, M. Montecchi, B.P. Doyle, E. Carleschi, and L. Pasquali, "Understanding adhesion of gold conductive films on sodium-alginate by photoelectron spectroscopy," Thin Solid Films **690**, 137535 (2019).
63. P. Slepička, Z. Kolská, J. Náhlík, V. Hnatowicz, and V. Švorčík, "Properties of Au nanolayers on polyethyleneterephthalate and polytetrafluoroethylene," Surf. Interface Anal. **41**(9), 741–745 (2009).
64. M. N. M. N. Perera, D. Schmidt, W. E. K. Gibbs, S. Juodkazis, and P. R. Stoddart, "Effective optical constants of anisotropic silver nanoparticle films with plasmonic properties," Opt. Lett. **41**(23), 5495–5498 (2016).
65. O. Arteaga, "Useful Mueller matrix symmetries for ellipsometry," Thin Solid Films **571**, 584–588 (2014).
66. B. G. McMillan, L. E. A. Berlouis, F. R. Cruickshank, D. Pugh, and P.-F. Brevet, "Transverse and longitudinal surface plasmon resonances of a hexagonal array of gold nanorods embedded in an alumina matrix," Appl. Phys. Lett. **86**(21), 211912 (2005).